Highly Efficient Electrochemical Nitrate and Nitrogen Reduction to Ammonia under Ambient Conditions on Electrodeposited Cu-Nanosphere Electrode

Giang Binh Truong,[a, b, c] Hung Tuan Duong,[a] Loi Duc Vu,[d] and Thao Thi Huong Hoang*[a]

The electrochemical reduction reaction of nitrogenous species such as NO_3^- (NO_3RR) and N_2 (NRR) is a promising strategy for producing ammonia under ambient conditions. However, low activity and poor selectivity of both NO_3RR and NRR remain the biggest problem of all current electrocatalysts. In this work, we fabricated Cu-nanosphere film with a high surface area and dominant with a Cu(200) facet by simple electrodeposition method. The Cu-nanosphere film exhibits high electrocatalytic activity for NO_3RR and NRR to ammonia under ambient conditions. In the nitrate environment, the Cu-nanosphere electrode reduced NO_3^- to yield NH_3 at a rate of 5.2 mg/h cm^2, with a Faradaic efficiency of 85% at -1.3 V. In the N_2-saturated environment, the Cu-nanosphere electrode reduced N_2 to yield NH_3 with the highest yield rate of 16.2 µg/h cm^2 at -0.5 V, and the highest NH_3 Faradaic efficiency of 41.6% at -0.4 V. Furthermore, the Cu-nanosphere exhibits excellent stability with the NH_3 yield rate, and the Faradaic efficiency remains stable after 10 consecutive cycles. Such high levels of NH_3 yield, selectivity, and stability at low applied potential are among the best values currently reported in the literature.

Introduction

Ammonia (NH_3) is one of the most produced chemicals in the world.[1] NH_3 is not only critically important for agriculture and industry but also a promising candidate for the carbon-free carrier of hydrogen energy that utilizes ammonia in fuel cells.[1–2] N_2 is an excellent nitrogen source to artificially convert to NH_3, due to the high abundance of N_2 in the atmosphere. However, breaking the N≡N triple bond in N_2, one of the most thermodynamically stable bonds in chemistry, is an enormous challenge in terms of energy. Current artificial NH_3 synthesis relies heavily on the well-known Haber-Bosch process (N_2+ $3H_2 \rightarrow 2NH_3$), which requires harsh synthesis conditions of high temperature (400–600 °C) and high pressure (200–250 bar). Consequently, this process consumes a large amount of energy (1–2% of global energy consumption) and releases a large quantity of CO_2 into the atmosphere (1.5 tons of CO_2 per ton of NH_3).[2–3]

A tremendous amount of effort has been invested in developing more economical and sustainable routes for NH_3 production, such as electrochemistry,[4] photochemistry,[5] and biological nitrogenase.[6] Among them, the electrochemical reduction reaction of nitrogenous species, including N_2 (NRR) and NO_3^- (NO_3RR), has recently attracted considerable attention because it can easily operate at room temperature and atmospheric pressure conditions.[4c,7] Moreover, the electrochemical reduction of nitrogenous species can utilize electricity produced from intermittent renewable energy resources without using fossil fuels and producing greenhouse gas. However, the main problems of NRR and NO_3RR are the sluggish kinetics and the highly competitive hydrogen evolution reaction (HER), leading to low activity and poor selectivity of nitrogenous species reduction.[4c,d] Thus, efficient catalysts remarkably increase the NH_3 yield rate while simultaneously suppressing the HER are urgently required.

Many metals and alloys, such as Pt,[8] Ni,[8a] Cu,[8–9] CuPt,[10] CuNi,[11] CuPb,[11] SnPd,[12]… have been investigated for the electrochemical reduction of nitrate NO_3RR. The products of this reduction process heavily rely on the characteristics of the electrode material. These products may include environmentally friendly nitrogen molecules (N_2) that are non-toxic, beneficial compounds like ammonium cation (NH_4^+), or even more hazardous substances than nitrate itself, such as nitrite (NO_2^-) and nitrogen oxides (NO, NO_2, N_2O).[13] Recently, Cu-nanosheets were reported with high Faradaic efficiency (FE) of 99.7% at a low overpotential of -0.15 V versus RHE.[14] Single-atom catalysts, such as Cu-N-C-SAC[15] and Fe-SAC[16] were reported with high NH_3 yield rate of 4.5 mg/cm^2.h and 7.8 mg/cm^2.h, respectively.

[a] G. B. Truong, Dr. H. T. Duong, Dr. T. T. H. Hoang
Institute of Chemistry
Vietnam Academy of Science and Technology
Hanoi 100000 (Vietnam)
E-mail: huongthao@ich.vast.vn

[b] G. B. Truong
Graduate University of Science
and Technology
Vietnam Academy of Science and Technology
Hanoi 100000 (Vietnam)

[c] G. B. Truong
School of Natural Sciences Education
Vinh University
Vinh City 43100, Nghean (Vietnam)

[d] Prof. Dr. L. D. Vu
Vietnam-Korea Institute of Science and Technology
Hanoi 100000 (Vietnam)

EurJIC
European Journal of Inorganic Chemistry

Research Article
doi.org/10.1002/ejic.202300371

Chemistry Europe
European Chemical Societies Publishing

From the energy point of view, the dissociation energy of the N=O in nitrate (204 kJ/mol) is significantly lower than the N≡N in nitrogen, thus nitrate is easier to be reduced to form NH_3 than nitrogen.[17] Despite that, researchers continue to make every effort to improve the electrosynthesis of NH_3 from N_2, which is more abundant than NO_3^-. Precious metals, such as Au,[18] Ru,[19] exhibit excellent electrocatalytic NRR activity. For example, a ruthenium/carbon black gas diffusion has recently been reported to exhibit record-high NRR activity up to 60.59 µg/h cm² NH_3 yield rate and 64.8% FE at relatively low potential (−0.1 V vs. RHE)[19c]. However, the high cost of these precious metals impedes their widespread application for NRR. To address this issue, many transition metal materials and metal-free materials, such as NiO,[20] MoS_2,[21] Fe_2O_3/Cu,[22] CuO,[23] C-ZIF,[24] Mo-FeP[25] have been developed as promising electrocatalysts for NRR.

As an abundant and low-cost material, Cu has been extensively studied for many electrocatalysis applications, such as supercapacitors,[26] fuel cells,[27] and CO_2 reduction.[28] Among many transition metals, copper was also proposed as a suitable electrode material for NO₃RR and NRR to form NH₃.[8a,9,22–23] Recently, a Cu-nanoporous material has been reported to exhibit extraordinary catalytic activity for CO_2 reduction (CRR).[28b] Since the CRR is somewhat analogous to NO₃RR and NRR, particularly all of them must compete with HER during the electrolysis. Thus, we hypothesize that an excellent CRR electrocatalyst that can effectively suppress HER and activate CRR, could also be a good NO₃RR and NRR catalyst.

Inspired by the above considerations, we focus on fabricating Cu-nanosphere film with a high surface area by simple electrodeposition method for the active and selective electroreduction of NO₃RR and NRR to ammonia. Remarkably, the Cu-nanosphere film exhibits electrocatalytic activity and stability among the best catalyst for NO₃RR and NRR.

Results and Discussion

Fabrication and Characterization of Cu-Nanosphere

Cu-nanosphere was prepared by electrodeposition with the presence of deposition additive 3,5-diamino-1,2,4-triazole. The mechanism by which 3,5-diamino-1,2,4-triazole modifies the morphology of the deposition film can be explained by a diffusion-limited aggregation process, similar to the other metal films electrodeposited with 3,5-diamino-1,2,4-triazole additive reported recently.[28–29] Here, 3,5-diamino-1,2,4-triazole acts as an electrodeposition inhibitor that binds to the surface, thus inhibiting surface diffusivity, then initiating roughness and forming abnormal morphology of the deposited film.[28b] Previous reports showed that the morphology of the electro-deposited film in the presence of 3,5-diamino-1,2,4-triazole strongly depends on pH, deposition current density, and substrate.[28b] In this work, the electrodeposition condition is chosen at a constant current density of 4.5 mA/cm², at pH = 2, on Cu substrate to control the well-defined morphology of the Cu film. The SEM (Figure 1b) and optical image (Figure S1b)
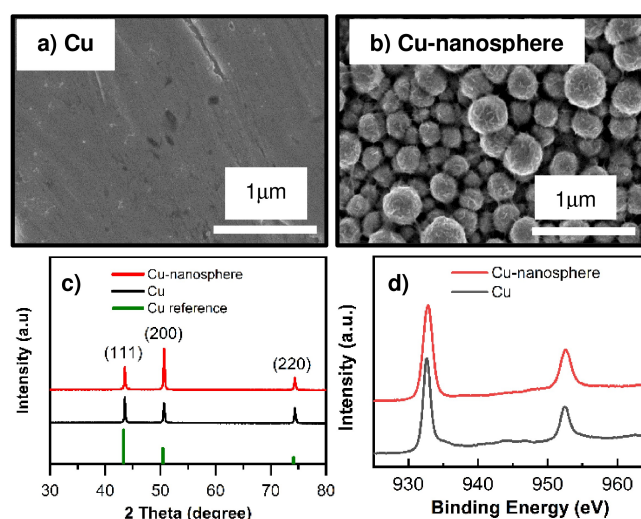
Figure 1. SEM images of a) Cu and b) Cu-nanosphere; c) XRD patterns; and d) XPS patterns of Cu and Cu-nanosphere.

show that the Cu-nanosphere exhibits a dull black surface with particles of a well-defined sphere shape. In contrast, the bare Cu plate exhibits a smooth (Figure 1a) and shiny metallic surface with red-copper color (Figure S1a), as normal.

The active surface area of the Cu and Cu-nanosphere electrode were measured by using the Pb underpotential deposition method (Pb UPD) (Figure S6). The result shows that the Cu plate exhibits roughness values similar to those from polycrystalline Cu reported before. Alternatively, the Cu-nanosphere electrode exhibits 5.7 times higher active surface area than the Cu plate (Table S1).

The XRD patterns of both Cu and Cu-nanosphere (Figure 1c) show the characteristic of metallic polycrystalline Cu with Cu (111) peak at 43.29°, Cu (200) peak at 50.43°, and Cu (220) peak at 74.13°. XRD pattern of Cu plate exhibits the dominant appearances of (111) facet similar to the standard pattern of Cu (JCPDS 00-004-0836). Interestingly, the XRD pattern of Cu-nanosphere exhibits the dominant appearances of (200) facet compared to the Cu plate and Cu standard reference. The XPS patterns (Figure 1d) also confirm the metallic characteristic of both Cu and Cu-nanosphere.

Electrocatalytic activity for NO₃RR of Cu-nanosphere

To evaluate the electrocatalytic activity of Cu-nanosphere for reduction reaction of nitrogenous species, we first conducted electrochemical NO₃RR in a two-compartment H-cell (Figure 2a). The anodic and cathodic compartments were separated by a Nafion-117 proton exchange membrane to avoid the oxidation of products at the anode. The main reaction at the anode is the oxygen evolution reaction:

$$(OER) \quad 2H_2O \rightarrow O_2 + 4H^+ + 4e^- \tag{1}$$
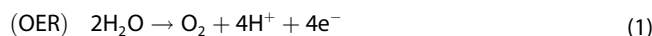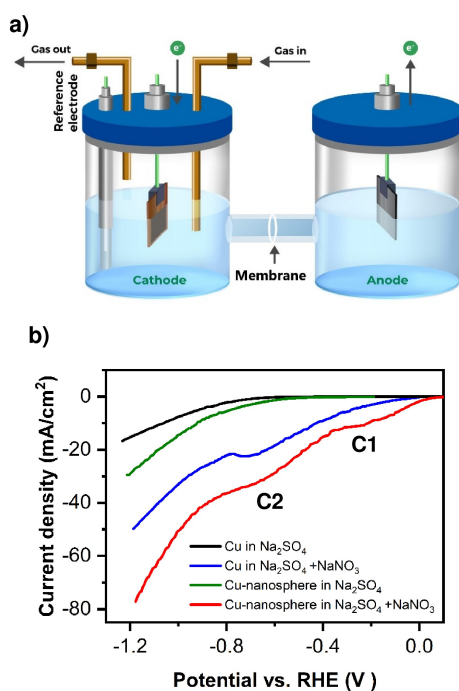
Figure 2. a) Schematic of two-compartment electrochemical cell, b) LSV in Na_2SO_4 with and without $NaNO_3$ of Cu and Cu-nanosphere.

The reactions at the cathode are nitrate reduction reactions (NO_3RR), and hydrogen evolution reactions (HER). It is widely accepted that the major products of NO_3RR on copper are NO_2^-, NH_4^+, and H_2; while N_2, NH_2OH, other NOx products probably are minor or not involved in the NO_3RR of copper:

$$(NO_3RR) \quad NO_3^- + H_2O + 2e^- \rightarrow NO_2^- + 2OH^- \quad (2)$$

$$NO_2^- + 6H_2O + 6e^- \rightarrow NH_4^+ + 7OH^- \quad (3)$$

$$(HER) \quad 2H^+ + 2e^- \rightarrow H_2 \quad (4)$$
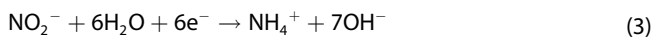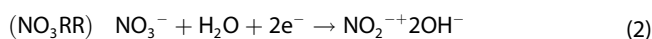
Figure 2b shows LSV curves of Cu and Cu-sphere electrodes in 0.5 M Na_2SO_4 with and without 0.1 M $NaNO_3$ at 10 mV/s scan rate. All the reduction current increase along with the negative shifting of applied potential. The reduction currents in Na_2SO_4 without $NaNO_3$ are associated with water reduction to H_2. The reduction currents in Na_2SO_4 with $NaNO_3$ are associated with NO_3^- reduction and H_2 evolution.

Figure 2b shows that the Cu and Cu-nanosphere exhibit higher electrochemical activity in electrolyte containing $NaNO_3$ (blue and red line) than in electrolyte without $NaNO_3$ (black and green line). The onset potential of reduction in electrolyte containing $NaNO_3$ is at ~0.0 V, while the onset potential in electrolyte without $NaNO_3$ is at ~−0.6 V. The electrodes in Na_2SO_4 with $NaNO_3$ exhibit ~2.5 times higher current density than in Na_2SO_4 without $NaNO_3$. This data suggests that NO_3^- is reduced and significantly contributed to the reduction current at potential < 0.0 V.

While the LSV of the electrodes in Na_2SO_4 without $NaNO_3$ shows smooth cathodic sweeps due to the evolution of only

one product H_2, the LSV in Na_2SO_4 with $NaNO_3$ shows wavy peaks at ~−0.2 V (C1) and ~−0.6 V (C2) due to the formation of different reduction products. It is widely accepted that C1 represents NO_3^- reduction to NO_2^- (equation 2), C2 represents NO_2^- reduction to NH_4^+ (equation 3).[30,31] Other products are still formed but without clear reduction peaks.

Figure 2b also shows that Cu nanosphere exhibits higher electrocatalytic activity than bare Cu. The onset potential of Cu nanosphere is about 0.1 V earlier than that of Cu. The current density of Cu nanosphere is about 1.5 times higher than that of Cu. The increased activity of the Cu-nanosphere compared to the Cu might be explained by the nanosphere morphology and the increase in the active surface area of the catalysts. The nanosphere structure exposes more active sites for electrochemical reduction than a flat surface.

To evaluate NH_3 yield during the NO_3RR, we also performed chronoamperometry (CA) tests at different potentials on Cu and Cu-nanosphere electrodes in $Na_2SO_4 + NaNO_3$ electrolyte for 1 hour at different potentials. Figure 3a shows that the Cu-nanosphere exhibits a higher reduction current density than the Cu at all potential. This current density data from the chronoamperometry method is consistent with the one from the LSV method described above (Figure 2b).

Figure 3b shows that the NH_3 FE of Cu and Cu-nanosphere increases with the potential being more negative. The NH_3 FE of Cu starts from ~3% at −0.1 V and reaches ~75% at −1.3 V NH_3; the NH_3 FE Cu-nanosphere starts from ~4% at −0.1 V and reach ~85% at −1.3 V NH_3. These data prove that NO_3RR to form NH_3 occurs at all potentials above −0.1 V. While the NH_3 FE of Cu and Cu-nanosphere are somewhat similar, the NH_3 yield of Cu-nanosphere is higher than of Cu (Figure 3c). At −1.3 V, the NH_3 yield of Cu-nanosphere reaches 5.2 mg/h.cm², which is ~2 times higher than of Cu. This data suggests that electrocatalytic activity for NO_3RR of Cu-nanosphere is higher than that of Cu electrode.
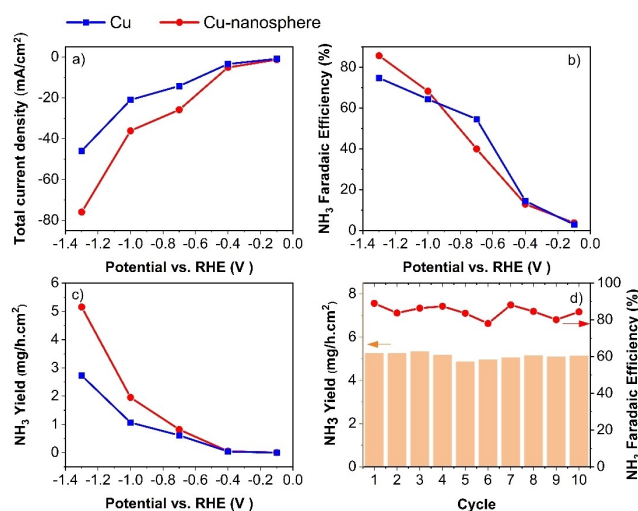
Figure 3. a) Total reduction current at corresponding potentials, b) Faradaic efficiency (FE) of NH_3 formation, c) NH_3 yield rate, and d) Stability test of Cu-nanosphere of NO_3RR at −1.3 V in 0.5 M $Na_2SO_4 + 0.1$ M $NaNO_3$ solution.

EurJIC
European Journal of Inorganic Chemistry

Research Article
doi.org/10.1002/ejic.202300371

Chemistry Europe
European Chemical Societies Publishing

To evaluate the durability of Cu-nanosphere, CA tests are performed at −1.3 V for 10 consecutive cycles. Figure 3d shows that the Cu-nanosphere exhibits excellent stability with NH₃ yield rate and FE remains almost the same after 10 cycles (~98% performance retention). This high stability for NO₃RR of Cu-nanosphere film could originate from its fabrication method. The Cu-nanosphere film was prepared by electrodeposition method on a bare Cu electrode, which does not require any binder to glue nanoparticles to the substrate. This self-supported structure of Cu-nanosphere enables the catalytic and conductive integrity of the catalyst, resulting in the enhancement of charge transfer and the improvement of catalyst stability.[28b,29,32]

[15]N isotope labeling experiments were conducted to confirm that the detected ammonia in NO₃RR experiment indeed originated from nitrate (Figure S7). The ¹H NMR spectra of the electrolytes after the reduction of ¹⁵NO₃⁻ showed double peaks with a spacing of ~73 Hz associated with ¹⁵NH₄⁺, consistent with the spectrum of standard reference ¹⁵NH₄⁺, and previous reports.[15,33] Conversely, the ¹H NMR of ¹⁴NH₄⁺ is split into three peaks with a smaller spacing of ~52 Hz.[33b] This result confirmed that the formation of ammonia originated from the electro-reduction of nitrates and ruled out contamination from N₂ gas, chemicals, lab environment, and catalyst.

Electrocatalytic Activity for NRR of Cu-nanosphere

To evaluate the electrocatalytic activity of Cu-nanosphere catalyst for NRR, LSV is conducted in a two-compartment H-cell. The reactions at the cathode are HER, and nitrogen reduction reaction:
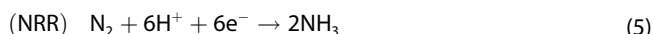
$$(\text{NRR}) \quad N_2 + 6H^+ + 6e^- \rightarrow 2NH_3 \tag{5}$$

Figure 4 shows LSV curves of Cu and Cu-nanosphere electrodes in Ar- and N₂-saturated 0.5 M Na₂SO₄ at a scan rate of 10 mV/s. All the reduction current increase along with the negative shifting of applied potential. The reduction currents in Ar-saturated environment are associated with HER. The reduction currents in N₂-saturated environment are associated with HER and NRR.[4c]
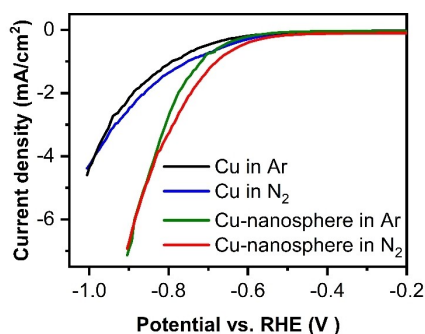
Figure 4 shows that the Cu exhibits low activity in this potential reaction in both Ar and N₂ environments. In contrast, the Cu-nanosphere exhibits much higher reduction currents and earlier onset than the Cu. The increased NRR activity of the Cu-nanosphere compared to the Cu, might be explained by the nanosphere morphology and the increase in the active surface area of the catalysts, as explained for NO₃RR. In particular, the current density of the Cu-nanosphere is ~3.5 times larger than that of Cu. The increase of current density is consistent with the Pb UPD measurement, where the active surface of Cu-nanosphere is 5.7 times larger than that of Cu. The small mismatch here may be because Pb²⁺ diffusion toward and into a porous electrode is easier than N₂ diffusion. Besides, this mismatch could also suggest that the current densities are dependent not only on the electrode surface area.

Figure 4 also shows that the Cu and Cu-nanosphere exhibit higher current density in N₂-saturated environment than in Ar. The significant difference in the LSV curves of N₂ and Ar is found at the potential from −0.4 V to −0.8 V. This data suggests that the N₂ reduction occurs at this potential range and contributes to the total reduction currents, or at least the presence of N₂ enhances the HER. As the potential being more negative than −0.8 V, there is no further difference in current density between Ar- and N₂-saturated environment on both electrodes. This data suggests that above −0.8 V, the HER is the only reaction; or NRR and HER compensate for each other, giving no increment in current density. This phenomenon is similar to NRR of other materials reported previously.[18a,20,34]

To evaluate the yield of NH₃ during the reduction reaction, we also performed chronoamperometry tests at different potentials on Cu and Cu-nanosphere electrodes in the N₂-saturated environment. Figure 5a shows that the Cu-nanosphere exhibits a higher reduction current density than the Cu at potential steps from −0.4 V to −0.8 V, especially at −0.7 V and −0.8 V. This reduction current from the CA is consistent with the one from the LSV described above (Figure 4).

Figure 4. LSV in and Ar- and N₂-saturated environments in Na₂SO₄ of Cu and Cu-nanosphere electrodes.
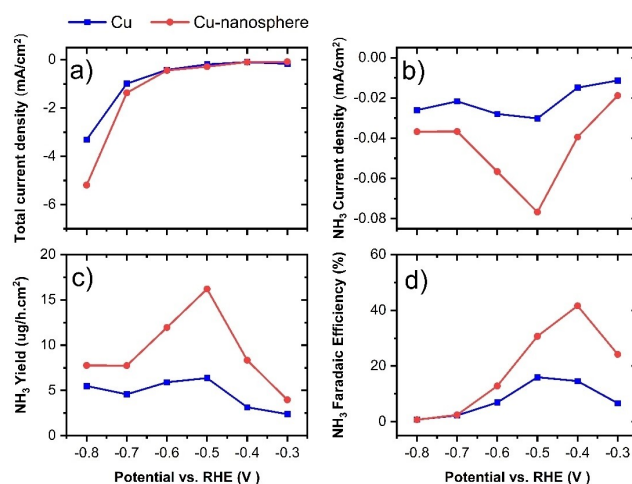
Figure 5. a) Total reduction current at corresponding potentials, b) Partial current density, c) Yield rate, and d) Faradaic efficiency of NH₃ formation from NRR in N₂-saturated 0.5 M Na₂SO₄.

EurJIC
European Journal of Inorganic Chemistry

Research Article
doi.org/10.1002/ejic.202300371

Chemistry
Europe
European Chemical
Societies Publishing

The rate of NH_3 formation is presented in Figures 5b and 5c in terms of NH_3 partial current density (mA/cm^2) and NH_3 yield rate ($\mu g/h \cdot cm^2$), respectively. Figures 5b and 5c show that both the absolute value of partial current density and the yield rate of NH_3 formation is larger than 0 at all potential steps from -0.3 V to -0.8 V. These data prove that NRR occurs at all potentials from -0.3 V to -0.8 V. Even at -0.8 V, where there is no significant difference between current density in the LSV in the N_2 and Ar environment (Figure 4), the NRR still occurs but at a relatively small rate. The rate of NH_3 formation of Cu-nanosphere is higher than that of Cu at all potentials, suggesting that electrocatalytic activity for NRR of Cu-nanosphere is higher than that of Cu.

The NH_3 yield rate of Cu and Cu-nanosphere increases with the potential being more negative and reaches maximum values at -0.5 V. While the NH_3 yield rate of Cu remains at this level even at more negative potentials, the NH_3 yield rate of Cu-nanosphere decreases significantly with more negative potential. A possible explanation for this trend is that the competing HER at the high negative potential that hinders the effective adsorption of N_2 on the catalyst surface shows more effect on the Cu-nanosphere with a rough and porous surface than on the Cu with a smooth surface. The maximum NH_3 yield rate of Cu-nanosphere is 16.2 $\mu g/h \, cm^2$, which is ~2.5 times higher than that of bare Cu (6.4 $\mu g/h \, cm^2$).

Figure 5d shows that the NH_3 FE of Cu and Cu-nanosphere increases with the potential being more negative. While the NH_3 FE of Cu reaches a maximum value of 16.0% at -0.5 V, the FE of Cu-nanosphere reaches a maximum value of 41.6% at a smaller potential of -0.4 V. At more negative potential, the NH_3 FE of both Cu and Cu-nanosphere decreases considerably and reaches ~0.7% at -0.8 V, which suggests that HER is the dominant reaction at the cathode. When the HER being dominant, most electrons and protons go toward reducing H_2O to H_2 instead of reducing N_2 to ammonia, resulting in low NH_3 FE[4c]. The dominance of HER at high negative potentials also explains the similar reduction current observed in LSV in N_2 and in Ar of both Cu and Cu-nanosphere electrodes at potentials beyond -0.8 V (Figure 4).

In addition, N_2H_4, a major by-product in the Haber-Bosch NH_3 synthesis process is not detected at all potentials of electrosynthesis of NH_3 from N_2, proving that Cu-nanosphere exhibits excellent NRR selectivity.

Interestingly, the XRD data (Figure 1c) show that the Cu-nanosphere is dominant with Cu(200), while normal Cu is dominant with Cu(111). Recently, Koper's group reported that the Cu(111) facet exhibits high activity toward the HER; also the inhibition and deactivation by adsorbed hydrogen on the Cu(111) facet lead to inefficient of NO_3RR.[30] Also, Wang's group reported experiments and DFT calculation proving that Cu film dominant with Cu(200) exhibits an efficient NO_3RR catalyst toward ammonia than Cu(111).[35] Therefore, the excellent NH_3 yield rate and Faradaic efficiency of the Cu-nanosphere film for NO_3RR and NRR could originate from the dominance of the Cu(200) facet of the material, despite the reaction mechanism of NO_3RR is quite different with NRR. Recently, new electrode materials with tailored facets have become a hot-spot in the field of electrochemical energy storage devices, many materials with specific tailored facets had been reported with high electrochemical activities.[36] However, the mechanism for the enhancement of electrochemical performances of our Cu-nanosphere, and others still require more detailed studies.

For most NRR catalysts, higher FE are obtained at relatively low potential and small current densities, leading to small NH_3 yield rate. However, high current density and high yield rate usually lead to small FE because the electrocatalyst surface is dominated by HER leaving no available active sites for NRR.[4c] Only few catalysts can provide good performance for both Faradaic efficiency and yield rate (Table S2).[18b,19b,34] It is clear that our Cu-nanosphere exhibits outstanding FE (41.6%) and relatively high NH_3 yield rate (16.2 $\mu g/h \, cm^2$) compared to other NRR electrocatalysts reported so far.

The data shows that Cu-nanosphere exhibits excellent catalytic activity with high NH_3 yield rates for both NO_3RR and NRR, interestingly the NH_3 yield of NO_3RR is much higher than that of NRR. Particularly, the highest NH_3 yield rate of NRR is 16.2 $\mu g/h \, cm^2$ at -0.5 V. While at the same range of potential, the NH_3 yield rate of NO_3RR is 51.9 $\mu g/h \, cm^2$, and the highest NH_3 yield rate of NO_3RR is up to 5.2 $mg/h \, cm^2$. This difference between the NH_3 yield rate of NO_3RR and NRR originates from the fact that nitrogen gas (N_2) is very stable due to its $N \equiv N$ triple bond (941 kJ/mol). Thus, converting N_2 into NH_3 through artificial means is extremely challenging in terms of energy. On the other hand, nitrate ions (NO_3^-) have advantages for ammonia synthesis due to their solubility and the relatively low dissociation energy of the $N=O$ bond (204 kJ/mol). This lower energy barrier favors the kinetics of the NO_3RR to form ammonia more feasible than the NRR.[37] Figure 3 shows that NO_3RR forms NH_3 at all steps of potential above -0.1 V, up to -1.3 V, and highly likely keep forming NH_3 at higher potential. While Figure 5 shows that the effective potential range of NRR to yield NH_3 is from -0.3 V to -0.7 V, at -0.8 V the FE of NH_3 is down to ~0%. This data once again confirms that the reduction of nitrate to ammonia is easier than of nitrogen to ammonia.

The LSV (Figures 2 and 4) and CA (Figures 3a, and 5a) show that the electrochemical behavior of Cu and Cu nanosphere are similar, yet the Cu nanosphere exhibits higher current densities. The NH_3 yield (figure 3b,c, 5b,c) shows that the product formation of Cu and Cu nanosphere are similar, yet the Cu nanosphere exhibits a higher yield rate. These data suggest that the mechanism of NO_3RR and NRR on Cu nanosphere are somewhat similar to Cu. The mechanism of NO_3RR and NRR on Cu electrodes was studied and reported in many other papers.[15,30,33a,38] The morphology, electrochemical active surface area, and crystal structure of the Cu nanosphere (Figure 1) suggested that the excellent NH_3 yield rate and NH_3 Faradaic efficiency of the Cu-nanosphere film originate from the high surface area and the dominance of the (200) facet of the material.

To further verify that NH_3 is generated from the electrochemical N_2 reduction of Cu-nanosphere, extensive control experiments and control conditions are carried out[39]. The amount of NO_3^-, NO_2^-, and NH_4^+ in the electrolyte was determined to confirm that no nitrogen source contamination

in the media could produce NH_3. The N_2 and Ar gases with ultrahigh purity (99.999%) were tested to guarantee no contamination of NO_x or NH_3 in the feed gases. The electrolysis of Cu-nanosphere with Ar gas under a condition similar to those in Figure 5, excepting using Ar gas instead of N_2 gas, was carried out to confirm that NH_3 formation is not due to the sources of contamination, such as electrochemical cell, membrane, electrodes. The control experiment of Cu-nanosphere in N_2 gas with no potential applied (open circuit potential) was carried out to confirm that NH_3 formation is not a spontaneous process; the NRR only occurs under appropriate potentials. Figure 6a shows that the yield of NH_3 is negligible before the electrolysis, after the electrolysis under Ar environment, and at OCP with no electrolysis. These data prove that the NH_3 is solely generated via the electrochemical reduction of N_2 to NH_3 on Cu-nanosphere.

^{15}N isotope labeling experiments were conducted to confirm that the detected ammonia in NRR experiments indeed originated from nitrogen (Figure S7). The ^1H NMR spectra of the electrolytes after the reduction of $^{15}N_2$ showed double peaks associated with $^{15}NH_4^+$.[15,33] This result confirmed that the formation of ammonia originated from the electroreduction of nitrogen and ruled out contamination from other sources.

To evaluate the durability of Cu-nanosphere, chronoamperometry tests are performed at the potential of maximum FE -0.4 V for 10 consecutive cycles. Figure 6b shows that the Cu-nanosphere exhibits excellent stability with small decreases in NH_3 yield rate (~85% performance retention), but the FE remains somewhat the same after 5 cycles. This high stability for NRR of Cu-nanosphere film could originate from self-supported structure of the electrodeposited Cu-nanosphere, as explained above. XRD and XPS pattern (Figure 6c, 6d) show that Cu-nanosphere retains metallic property and (200) facet dominance after the electrolysis experiments. This data suggests that the Cu-nanosphere film is stable on the electrode even after

vigorous bubbling gas and products evolution of the electrolysis.

Conclusions

In summary, Cu-nanosphere film with a high surface area was successfully deposited on a bare Cu substrate by electrodeposition method. The self-supported nanosphere structure of the Cu-nanosphere film enabled the exposure of more active sites for electrochemical reduction, leading to higher electrochemical activity than that of the flat Cu electrode. Electrochemical tests showed that the Cu-nanosphere film exhibits outstanding electrocatalytic activity for NO_3RR and NRR under ambient conditions. NH_3 yield rate for NO_3RR of the Cu-nanosphere is 5.2 mg/h.cm^2, with Faradaic efficiency of 85% at -1.3 V. The highest NH_3 yield rate on the Cu-nanosphere electrode (16.2 µg/h.cm^2) is achieved at -0.5 V, while the highest NH_3 Faradaic efficiency (41.6%) is achieved at -0.4 V. The excellent NH_3 yield rate and NH_3 Faradatic efficiency of the Cu-nanosphere film originate from high surface area and the dominance of the (200) facet of the material. The Cu-nanosphere also exhibits excellent performance and material stability after 5 consecutive cycles of electrolysis.

Experimental Section

Preparation of Cu-Nanosphere: The Cu-nanosphere film was electrodeposited at a constant current density of 4.5 mA on 1.0 cm^2 electrode for 500 seconds in a plating bath containing 0.1 M $CuSO_4 \cdot 5H_2O$ and 10 mM of 3,5-diamino-1,2,4-triazole, with the pH adjusted to 2 by using H_2SO_4. Polycrystalline Cu (99.99%) plate was used as the electrodeposition substrate. Cu plates were mechanically polished with sandpaper before being used to prepare a clean, flat, and uniform surface. Pt mesh was used as the counter electrode, separated from the working electrode by an ion exchange Nafion-117 membrane in a two-compartment electrochemical cell.

Materials Characterization: Scanning electron microscopy (SEM) images of Cu and Cu-nanosphere were obtained using a Hitachi S-4800 High Resolution Microscope. X-ray diffraction (XRD) patterns were recorded using a Bruker D8 Advance X-ray Diffractometer. X-ray photoelectron spectroscopy (XPS) was recorded using a Physical Electronics PHI 5400 instrument. The active surface area of the electrode was determined by the Pb underpotential deposition (UPD) method.

Electrochemical Measurements: The linear sweep voltammetry and the chronoamperometry were performed at room temperature using a Metrohm 797 VA potentiostat with a Cu or Cu-nanosphere as a working electrode, a Pt-mesh counter electrode, and an Ag/AgCl reference electrode. The Ag/AgCl reference electrode was calibrated before each experiment with a Reversible hydrogen electrode (RHE) in the study electrolyte. The working electrode was a Cu (99.99%) plate and Cu-nanosphere film deposited on a Cu plate. One side of the electrode was covered with epoxy resin for chemical resistance and electrical insulation, leaving only one side of the electrode in contact and reacting with the electrolyte. The counter electrode was separated from the working electrode by using a Nafion-117 membrane in a two-compartment electrochemical cell (Figure 1).
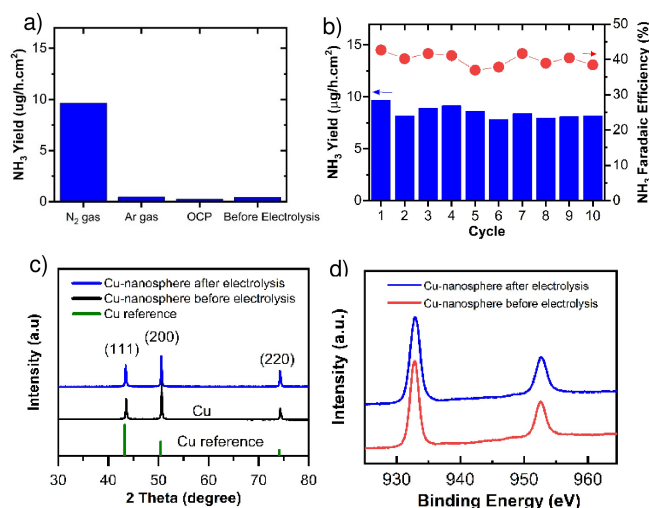
Figure 6. a) NH_3 yield rate of Cu-nanosphere in N_2 environment, Ar environment, at OCP with no electrolysis, and before the electrolysis; b) Stability test of NRR on Cu-nanosphere at -0.4 V for 10 consecutive cycles; c) XRD patterns; and d) XPS patterns of Cu-nanosphere before and after electrolysis.

EurJIC
European Journal of Inorganic Chemistry

Research Article
doi.org/10.1002/ejic.202300371

Chemistry
Europe
European Chemical
Societies Publishing

The electrolyte for NO_3RR was 0.5 M Na_2SO_4 + 0.1 M $NaNO_3$. The electrolyte for NRR was 0.5 M Na_2SO_4. The ultrahigh purity N_2 gas (99.999%) and Ar gas (99.999%) were purged into the electrolyte for 30 mins to obtain N_2 or Ar-saturated environment and remove other dissolved gases. The gases continued bubbling into the electrolyte to remain the saturated environment during the chronoamperometry measurement. During the LSV, the gases were kept flowing on top of the electrolyte to avoid penetration of outside gases into the chamber. LSV was carried out at scan rate of 10 mV/s, and the CA tests were operated for 1 hour at different potentials.

Determination of Electrolysis Products: The concentration of NH_3 was determined by an indophenol blue method.[40] The N_2H_4 concentration was determined by the Watt-Chrisp method.[41] The NO_2^- concentration was determined by the naphthyl-ethylenediamine method.[40] H_2 was determined by gas chromatography equipped with a column MolSieve 13X and a thermal conductivity detector. ^{1}H NMR spectra of [15]NH_4^+ generated from NO_3RR using $Na^{15}NO_3$ as reactant, and from NRR using [15]N_2 as reactant was performed at 25°C on a Bruker Ascend 600 MHz using DMSO-d6 solvent. See the supporting information for more detailed analysis procedure.

Supporting Information

Supporting Information have cited additional references.[33a,42]

Conflict of Interests

The authors declare no conflict of interest.

Data Availability Statement

The data that support the findings of this study are available from the corresponding author upon reasonable request.

[1] V. Rosca, M. Duca, M. T. De Groot, M. T. M. Koper, *Chem. Rev.* **2009**, *109*, 2209–2244.
[2] C. J. M. van der Ham, M. T. M. Koper, D. G. H. Hetterscheid, *Chem. Soc. Rev.* **2014**, *43*, 5183–5191.
[3] P. J. Chirik, *Nat. Chem.* **2009**, *1*, 520–522.
[4] a) R. Lan, J. T. S. Irvine, S. W. Tao, *Sci. Rep.* **2013**, *3*; b) S. M. Chen, S. Perathoner, C. Ampelli, C. Mebrahtu, D. S. Su, G. Centi, *Angew. Chem. Int. Ed.* **2017**, *56*, 2699–2703; c) G. Qing, R. Ghazfar, S. T. Jackowski, F. Habibzadeh, M. M. Ashtiani, C. P. Chen, M. R. Smith 3rd, T. W. Hamann, *Chem. Rev.* **2020**, *120*, 5437–5516; d) J. H. Montoya, C. Tsai, A. Vojvodic,

J. K. Norskov, *ChemSusChem* **2015**, *8*, 2180–2186; e) Z. Chen, C. L. Liu, L. C. Sun, T. Wang, *ACS Catal.* **2022**, *12*, 8936–8975; f) J. Liang, Z. Li, L. Zhang, X. He, Y. Luo, D. Zheng, Y. Wang, T. Li, H. Yan, B. Ying, S. Sun, Q. Liu, M. S. Hamdy, B. Tang, X. Sun, *Chem* **2023**, *9*, 1768–1827; g) Q. Liu, T. Xu, Y. Luo, Q. Kong, T. Li, S. Lu, A. A. Alshehri, K. A. Alzahrani, X. Sun, *Curr. Opin. Electrochem.* **2021**, *29*, 100766.
[5] a) K. A. Brown, D. F. Harris, M. B. Wilker, A. Rasmussen, N. Khadka, H. Hamby, S. Keable, G. Dukovic, J. W. Peters, L. C. Seefeldt, *Science* **2016**, *352*, 448–450; b) D. Zhu, L. Zhang, R. E. Ruther, R. J. Hamers, *Nat. Mater.* **2013**, *12*, 836–841.
[6] a) R. D. Milton, S. Abdellaoui, N. Khadka, D. R. Dean, D. Leech, L. C. Seefeldt, S. D. Minteer, *Energy Environ. Sci.* **2016**, *9*, 2550–2554; b) J. Kästner, P. E. Blöchl, *J. Am. Chem. Soc.* **2007**, *129*, 2998–3006.
[7] M. El-Shafie, S. Kambara, *Int. J. Hydrogen Energy* **2023**, *48*, 11237–11273.
[8] a) K. Bouzek, M. Paidar, A. Sadilkova, H. Bergmann, *J. Appl. Electrochem.* **2001**, *31*, 1185–1193; b) G. E. Dima, A. C. A. De Vooys, M. T. M. Koper, *J. Electroanal. Chem.* **2003**, *554*, 15–23.
[9] G. E. Badea, *Electrochim. Acta* **2009**, *54*, 996–1001.
[10] S. Kerkeni, E. Lamy-Pitara, J. Barbier, *Catal. Today* **2002**, *75*, 35–42.
[11] L. Li, Y. F. Yun, Y. Z. Zhang, Y. X. Huang, Z. H. Xu, *J. Alloys Compd.* **2018**, *766*, 157–160.
[12] Y. Y. Birdja, J. Yang, M. T. M. Koper, *Electrochim. Acta* **2014**, *140*, 518–524.
[13] a) G. Kreysa, K.-i. Ota, R. F. Savinell, *Encyclopedia of applied electrochemistry* **2014**; b) M. Duca, M. T. M. Koper, *Energy Environ. Sci.* **2012**, *5*, 9726–9742.
[14] X. B. Fu, X. G. Zhao, X. B. Hu, K. He, Y. N. Yu, T. Li, Q. Tu, X. Qian, Q. Yue, M. R. Wasielewski, Y. J. Kang, *Appl Mater Today* **2020**, *19*.
[15] J. Yang, H. F. Qi, A. Q. Li, X. Y. Liu, X. F. Yang, S. X. Zhang, Q. Zhao, Q. K. Jiang, Y. Su, L. L. Zhang, J. F. Li, Z. Q. Tian, W. Liu, A. Q. Wang, T. Zhang, *J. Am. Chem. Soc.* **2022**, *144*, 12062–12071.
[16] Z. Y. Wu, M. Karamad, X. Yong, Q. Z. Huang, D. A. Cullen, P. Zhu, C. A. Xia, Q. F. Xiao, M. Shakouri, F. Y. Chen, J. Y. Kim, Y. Xia, K. Heck, Y. F. Hu, M. S. Wong, Q. L. Li, I. Gates, S. Siahrostami, H. T. Wang, *Nat. Commun.* **2021**, *12*.
[17] X. Y. Liang, H. D. Zhu, X. X. Yang, S. S. Xue, Z. Z. Liang, X. F. Ren, A. M. Liu, G. Wu, *Small Structures* **2022**.
[18] a) M. Nazemi, S. R. Panikkanvalappil, M. A. El-Sayed, *Nano Energy* **2018**, *49*, 316–323; b) M. M. Shi, D. Bao, B. R. Wulan, Y. H. Li, Y. F. Zhang, J. M. Yan, Q. Jiang, *Adv. Mater.* **2017**, *29*.
[19] a) M. Kitano, S. Kanbara, Y. Inoue, N. Kuganathan, P. V. Sushko, T. Yokoyama, M. Hara, H. Hosono, *Nat. Commun.* **2015**, *6*; b) Z. Geng, Y. Liu, X. Kong, P. Li, K. Li, Z. Liu, J. Du, M. Shu, R. Si, J. Zeng, Adv. Mater. 2018, 30, 1803498; c) X. Wei, M. Pu, Y. Jin, M. Wessling, *ACS Appl. Mater. Interfaces* **2021**, *13*, 21411–21425.
[20] K. Chu, Y. P. Liu, J. Wang, H. Zhang, *ACS Appl. Energ. Mater.* **2019**, *2*, 2288–2295.
[21] L. Zhang, X. Q. Ji, X. Ren, Y. J. Ma, X. F. Shi, Z. Q. Tian, A. M. Asiri, L. Chen, B. Tang, X. P. Sun, *Adv. Mater.* **2018**, *30*.
[22] C. Huang, L. Shang, P. Han, Z. Gu, A. M. Al-Enizi, T. M. Almutairi, N. Cao, G. Zheng, *J. Colloid Interface Sci.* **2019**, *552*, 312–318.
[23] F. Wang, Y. P. Liu, H. Zhang, K. Chu, *ChemCatChem* **2019**, *11*, 1441–1447.
[24] K. Kim, C. Y. Yoo, J. N. Kim, H. C. Yoon, J. I. Han, *J. Electrochem. Soc.* **2016**, *163*, F1523-F1526.
[25] Y.-X. Luo, W.-B. Qiu, R.-P. Liang, X.-H. Xia, J.-D. Qiu, *ACS Appl. Mater. Interfaces* **2020**, *12*, 17452–17458.
[26] D. Dubal, D. Dhawale, R. Salunkhe, V. Jamdade, C. Lokhande, *J. Alloys Compd.* **2010**, *492*, 26–30.
[27] M. A. Thorseth, C. E. Tornow, C. Edmund, A. A. Gewirth, *Coord. Chem. Rev.* **2013**, *257*, 130–139.
[28] a) T. T. H. Hoang, S. Verma, S. C. Ma, T. T. Fister, J. Timoshenko, A. I. Frenkel, P. J. A. Kenis, A. A. Gewirth, *J. Am. Chem. Soc.* **2018**, *140*, 5791–5797; b) T. T. H. Hoang, S. C. Ma, J. I. Gold, P. J. A. Kenis, A. A. Gewirth, *ACS Catal.* **2017**, *7*, 3313–3321.
[29] T. T. H. Hoang, A. A. Gewirth, *ACS Catal.* **2016**, *6*, 1159–1164.
[30] E. Pérez-Gallent, M. C. Figueiredo, I. Katsounaros, M. T. Koper, *Electrochim. Acta* **2017**, *227*, 77–84.
[31] T. Y. Wu, X. G. Kong, S. Y. Tong, Y. Chen, J. Liu, Y. Tang, X. J. Yang, Y. M. Chen, P. Y. Wan, *Appl. Surf. Sci.* **2019**, *489*, 321–329.
[32] J. Liu, D. Zhu, Y. Zheng, A. Vasileff, S.-Z. Qiao, *ACS Catal.* **2018**, *8*, 6707–6732.
[33] a) Y. X. Lin, S. N. Zhang, Z. H. Xue, J. J. Zhang, H. Su, T. J. Zhao, G. Y. Zhai, X. H. Li, M. Antonietti, J. S. Chen, *Nat. Commun.* **2019**, *10*; b) D. Liu, M. P. Chen, X. Y. Du, H. Q. Ai, K. H. Lo, S. P. Wang, S. Chen, G. C. Xing, X. S. Wang, H. Pan, *Adv. Funct. Mater.* **2021**, *31*.

[34] W. J. Zang, T. Yang, H. Y. Zou, S. B. Xi, H. Zhang, X. M. Liu, Z. K. Kou, Y. H. Du, Y. P. Feng, L. Shen, L. L. Duan, J. Wang, S. J. Pennycook, *ACS Catal.* **2019**, *9*, 10166–10173.

[35] S. B. Patil, T.-R. Liu, H.-L. Chou, Y.-B. Huang, C.-C. Chang, Y.-C. Chen, Y.-S. Lin, H. Li, Y.-C. Lee, Y. J. Chang, *J. Phys. Chem. Lett.* **2021**, *12*, 8121–8128.

[36] F. X. Wang, X. W. Wang, Z. Chang, Y. S. Zhu, L. J. Fu, X. Liu, Y. P. Wu, *Nanoscale Horiz.* **2016**, *1*, 272–289.

[37] Q. Liu, L. S. Xie, J. Liang, Y. C. Ren, Y. Y. Wang, L. C. Zhang, L. C. Yue, T. S. Li, Y. S. Luo, N. Li, B. Tang, Y. Liu, S. Y. Gao, A. A. Alshehri, I. Shakir, P. O. Agboola, Q. Q. Kong, Q. Y. Wang, D. W. Ma, X. P. Sun, *Small* **2022**, *18*.

[38] X. D. Wang, M. Q. Zhu, G. S. Zeng, X. Liu, C. H. Fang, C. H. Li, *Nanoscale* **2020**, *12*, 9385–9391.

[39] a) L. Q. Li, C. Tang, D. Z. Yao, Y. Zheng, S. Z. Qiao, *ACS Energy Lett.* **2019**, *4*, 2111–2116; b) B. H. R. Suryanto, H. L. Du, D. B. Wang, J. Chen, A. N. Simonov, D. R. MacFarlane, *Nat. Catal.* **2019**, *2*, 290–296.

[40] E. W. Rice, R. B. Baird, A. D. Eaton, L. S. Clesceri, *Standard methods for the examination of water and wastewater, Vol. 10*, American public health association Washington, DC, **2012**, 4-114–4-125.

[41] G. W. Watt, J. D. Chrisp, *Anal. Chem.* **1952**, *24*, 2006–2008.

[42] a) P. Jing, P. Liu, M. Hu, X. Xu, B. Liu, J. Zhang, *Small* **2022**, *18*, e2201200; b) S. Mukherjee, D. A. Cullen, S. Karakalos, K. X. Liu, H. Zhang, S. Zhao, H. Xu, K. L. More, G. F. Wang, G. Wu, *Nano Energy* **2018**, *48*, 217–226.

RESEARCH ARTICLE

Cu-nanosphere film with a high surface area and dominant (200) facet was fabricated by a simple electrode-position method. The Cu-nanosphere achieved excellent nitrate reduction reaction (NO$_3$RR), and nitrogen reduction reaction (NRR) performance. The dominance of the Cu (200) facet of the Cu-nanosphere electrocatalyst suppresses the competing hydrogen evolution reaction (HER) and thus exhibits better electrochemical NO$_3$RR and NRR selectivity.
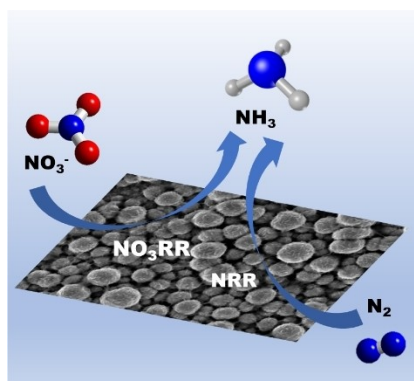
*G. B. Truong, Dr. H. T. Duong, Prof. Dr. L. D. Vu, Dr. T. T. H. Hoang**

1 – 9

Highly Efficient Electrochemical Nitrate and Nitrogen Reduction to Ammonia under Ambient Conditions on Electrodeposited Cu-Nanosphere Electrode